A HYBRID TECHNIQUE FOR AIRFOIL INVERSE DESIGN OF AXIAL FLOW TURBOMACHINE CASCADES USING CONFORMAL MAPPING AND THE PANEL METHOD

Denis Rinaldi Petrucci
Universidade Federal de Itajubá – Departamento de Engenharia Mecânica
Av. BPS 1303 – Itajubá, MG – 37500-903
denisrpetrucci@uol.com.br

Nelson Manzanares Filho
Universidade Federal de Itajubá – Departamento de Engenharia Mecânica
Av. BPS 1303 – Itajubá, MG – 37500-903
nelson@iem.efei.br

Abstract. In this paper a hybrid numerical technique for cascade airfoil design is presented. The technique consists in a suitable combination of a conformal mapping and a linear vortex panel method. The coordinates of a circle or quasi-circle in the transformed plane are searched in order to satisfy a required velocity distribution on the target airfoil contour at the physical plane. The velocity distribution is prescribed as a function of the natural coordinate. The geometrical marching is conducted by varying the panel slopes according to the normal velocity excess induced by the difference between the required and calculated velocities. A scheme is applied in order to close the body shape. The use of a conformal mapping increases the precision of the inverse procedure, by damping possible geometrical oscillations at the leading edge region caused by the panel slope variations during the iterative process. In this way, smooth aerodynamic shapes are guaranteed to be produced on the whole contour. Some test results are presented for a Weinig cascade, the Gostelow cascade and a cascade of Joukowski airfoils.

Keywords. *Inverse method, Conformal mapping, Panel method, Cascades, Turbomachines.*

1. Introduction

The problems involving aerodynamic computations can be classified in two major categories: 1) the direct problem, in which the whole geometry is known, as well as inlet or outlet flow angles, and the flow field distributions (velocity and pressure) are to be determined; 2) the inverse or design problem, in which some desired flow characteristic are furnished (such as pressure or velocity surface distributions), and the aerodynamic shapes are to be determined.

Yiu (1994) classified the aerodynamic shape design methods in four categories: 1) the inverse methods, based on iterative correction or solution of nonlinear equation systems; 2) iterative modification methods, including optimization techniques; 3) transformed plane methods, including conformal mapping and hodograph methods; 4) special methods, including panel methods for potential flow. It is possible to conceive some combinations in this classification. For instance, there are inverse methods based on conformal mapping techniques or integral formulations numerically solved by means of panel methods.

Liu (2000) identified four categories of aerodynamic design problems in an ascending order of complexity: 1) the direct problem; 2) the inverse problem; 3) the hybrid problem unifying and generalizing the two problems above, and for which some alternative solution procedures were proposed by Dulikravich (1992), Liu (1995) and Yiu (1994); 4) the optimization problem, where one is asked for optimum geometrical solutions in order to attain a certain objective, subjected to some restrictions (for example, a target airfoil with minimum drag-lift ratio, satisfying prescribed ranges of maximum camber and thickness).

Shigemi (1985) proposed an inverse design method for multielement airfoils using a straight panel method with linear vortex distributions and the Neumann boundary condition applied on the control points. The resulting nonlinear equation system was solved by the Newton-Raphson method with the airfoil ordinates as unknowns. A least square technique was applied for guaranteeing closed airfoil shapes and fixing the leading and trailing edges.

Selig and Maughmer (1992 a, b) presented a multipoint inverse method for airfoil design using a general conformal mapping. The airfoil surface was divided into various segments, each of them associated with a required velocity distribution and a corresponding angle of attack. The coordinates of the intersection points of the segments were unknowns calculated by means of the Newton-Raphson method. The method is capable to incorporate requirements of maximum camber and thickness as well as boundary layer criteria. The methodology was later extend by Selig (1994) for treating turbomachinery cascades.

Murugesan and Railly (1969) proposed an inverse design panel method for cascades, which represent an alternative to the Newton-Raphson method an other nonlinear equation solvers for iterative calculation of the airfoil coordinates. In each iteration, the method computes a distribution of normal velocities induced by the difference between the calculated and required velocities on the airfoil surface (as a fictitious vortex distribution). This distribution must be gradually annulated by varying the panel slopes until a converged shape is reached, satisfying the impenetrability condition.

Petrucci et al. (2001) presented a rapid inverse algorithm for airfoil design using a straight panel method with linear vortex distributions and applying the procedure of Murugesan and Railly (1969) for the iterative geometric correction.

Converged results were obtained with a relatively small number of iterations, but some drawbacks were also present. The principal of them was the introduction of an automatic filter on the fictitious vortex distribution for damping some spurious geometrical oscillations that could sometimes result at the leading edge region. Even so the method was not capable to avoid small geometric oscillations for all of the tested cases.

In this work, the inverse design method proposed by Petrucci ans Manzanares (2002) for isolated airfoils is extended to axial flow turbomachinery cascades. The method consists in a suitable combination of a conformal mapping and an efficient panel method based on linear vortex distributions (Petrucci et al., 2001). The coordinates of a circle or quasi-circle in the transformed plane are searched in order to satisfy a required velocity distribution on the target airfoil contour at the physical plane which is prescribed as a function of the natural coordinate. The geometrical marching is conducted by varying the panel slopes according to the normal velocity excess induced by the difference between the required and calculated velocities. The use of a conformal mapping increases the precision of the inverse procedure, by damping possible geometrical oscillations at the leading edge region caused by the panel slope variations during the iterative process. In this way, smooth aerodynamic shapes are guaranteed to be produced on the whole contour.

Various tests were carried out to validate the proposed methodology and some results are presented for three of them: a Weinig cascade, the Gostelow cascade and a cascade of Joukowski airfoils.

2. General Algorithm Description

The algorithm applies the Weinig conformal mapping (Fernandes, 1978) to represent the airfoil shape in the physical plane $z^*(x^*, y^*)$ from a circle or quasi-circle in the transformed plane $\zeta^*(\xi^*, \eta^*)$, as shown in Fig. 1. The potential flow is calculated in the transformed plane by means of a straight panel method based on linear vortex distributions (Petrucci et al., 2001). A required velocity distribution is given in the physical plane as a function of the natural airfoil coordinate. In the transformed plane, a starting circular shape is suitably chosen (section 3). An iterative process is thus carried out, by which the transformed shape is gradually modified in order to satisfy the required physical velocity, the impenetrability condition and the mapping relationships. Each iteration is subdivided into three steps: 1) an initial step in which some conformal mapping parameters are computed; 2) the flow calculation step, using the panel method in the transformed plane; after this step, a convergence criteria is checked; 3) the geometric marching step, if convergence is not attained yet. These steps are described in detail in the following sections.

The algorithm is essentially the same already described by Petrucci and Manzanares (2002 a) for isolated airfoils. The principal difference is the use of the Weinig conformal mapping in place of the Joukowski mapping, which is only a valid limit for cascades of large pitch chord ratios. The Weinig mapping transforms circles in airfoil cascades with any desired values of pitch and stagger. Another difference introduced in this paper is the use of a camber angle for displacing the transformed shape in each iteration in order to accelerate the convergence process for cambered airfoils.

3. Computation of conformal mapping parameters

Figure 1 illustrates the Weinig conformal mapping, by which a centered circle in the transformed plane $\zeta^*(\xi^*, \eta^*)$ is mapped on a flat plate cascade in the physical plane $z^*(x^*, y^*)$. If the circle is slightly displaced with respect to the critical points and the circular shape is also modified one can obtain any desired airfoil cascade in the physical plane. Here the forward critical point will be displaced to the interior of the transformed shape while the rear critical point will remain on the contour. In this way an airfoil with a rounded leading edge and a cusped trailing edge will be generated.
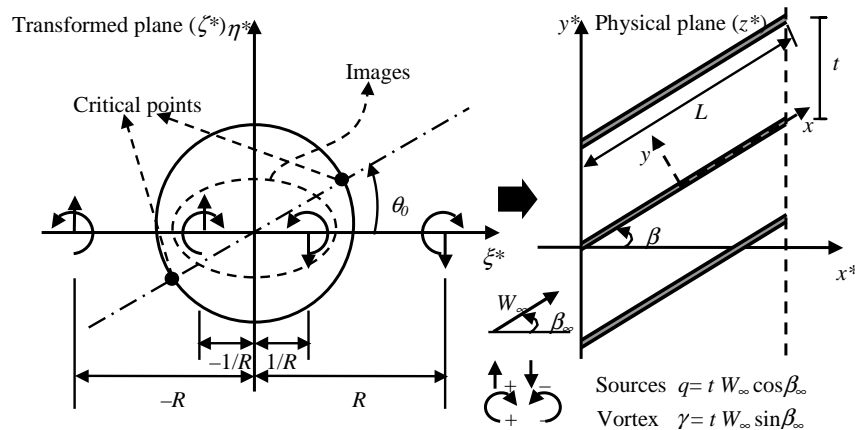

Figure 1. Conformal mapping of a flat plate cascade from a circle.

The physical and conformal mapping parameters are shown in Fig. 1. The geometric cascade parameters are the pitch t, the chord length L and the stager angle β. The corresponding mapping parameters are the circle radius c, the distance R between the circle center and the singularity locations (sources and vortex simulating the upstream and

downstream cascade flows) and the angle θ_0 of the critical points. β_∞ and W_∞ represent the angle and magnitude of the mean flow velocity in the physical plane . The Weinig transformation z^* (ζ^*) is given by:

$$z^* = \frac{t}{2\pi}\left[\log\left(\frac{R+\zeta^*}{R-\zeta^*}\right) + e^{2i\beta}\log\left(\frac{\zeta^* + c^2/R}{\zeta^* - c^2/R}\right)\right] \qquad (1)$$

It is convenient to work in a ζ transformed plane with the critical points intercepting the ξ abscissa axis. The airfoil trailing edge (cusped) will be located on the x abscissa of a physical plane $z(x, y)$, Fig. 2. The forward critical point will be located inside the circle or quasi-circle in order to obtain an airfoil with a rounded leading edge. Thus, one considers a larger circle of radius $a > c$ with its center displaced by a "camber angle" β^* with respect to the ξ abscissa . The rear critical point remains at $(c, 0)$.

Transformed plane (ζ)   Physical plane (z)

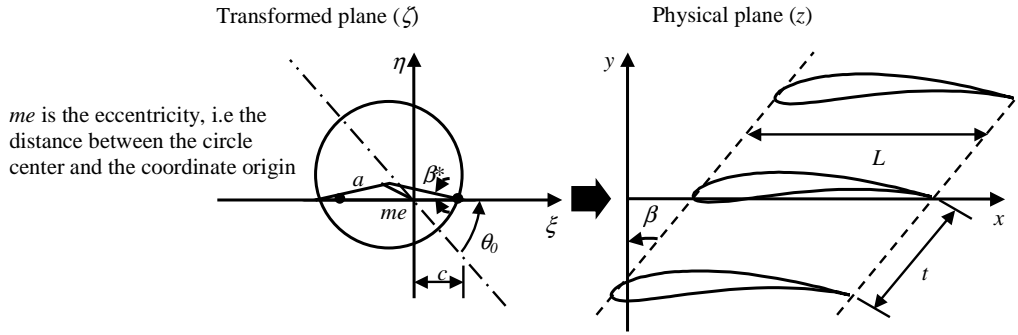me is the eccentricity, i.e the distance between the circle center and the coordinate origin

Figure 2. Conformal mapping of an airfoil cascade in the z plane from a circle in the ζ plane.

With the necessary considerations, the conformal mapping z (ζ) follows from Eq. 1:

$$z = \frac{t}{2\pi}\left[e^{-i\beta}\log\left(\frac{R+\zeta e^{i\theta_0}}{R-\zeta e^{i\theta_0}}\right) + e^{i\beta}\log\left(\frac{\zeta e^{i\theta_0} + c^2/R}{\zeta e^{i\theta_0} - c^2/R}\right)\right] \qquad (2)$$

where the parameters $\theta_0(L/t, \beta)$ and $R(L/t, \beta)$, are determined by solving the following system of two nonlinear algebraic equations:

$$\begin{cases} \tan\theta_0 = \tan\beta\,\dfrac{(R/c)^2 - 1}{(R/c)^2 + 1} & (3) \\[4mm] \dfrac{L}{t} = \dfrac{1}{\pi}\left[\cos\beta\ln\left(\dfrac{(R/c)^2 + 2(R/c)\cos\theta_0 + 1}{(R/c)^2 - 2(R/c)\cos\theta_0 + 1}\right) + 2\sin\beta\tan^{-1}\left(\dfrac{2(R/c)\sin\theta_0}{(R/c)^2 - 1}\right)\right] & (4) \end{cases}$$

To accelerate the converge towards the target physical airfoil, it is convenient to recalculate the parameters of a circle close to the quasi-circle in each iteration. Thus one begins with a relation between the geometrical parameters of the circle and the magnitude of trailing edge velocity, $|W_{te}|$, valid for a Joukowski airfoil (Milne-Thomson, 1966):

$$|W_{te}| = \frac{c \cdot W_\infty \cos(\alpha + \beta^*)}{a} \qquad (5)$$

For an airfoil in cascade it is convenient to adopt the following approximation, by replacing the incidence velocity magnitude W_∞ by the downstream velocity magnitude W_2:

$$|W_{te}| = \frac{c \cdot W_2 \cos(\alpha + \beta^*)}{a} \qquad (6)$$

For determining the "camber angle" β^* one considers the circulation around the target airfoil by integrating the required velocity distribution $W_{req}(s)$ around the contour (which is given):

$$\Gamma = \int W_{req}(s)\,ds \tag{7}$$

Considering a discrete distribution $W_{req\,i}$ given in $m+1$ nodal points of natural coordinates s_i, $i = 1,\ldots, m+1$, one has :

$$\Gamma \cong \sum_{i=1}^{m} \frac{W_{req_i} + W_{req_{i+1}}}{2}(s_{i+1} - s_i) \tag{8}$$

The lift coefficient of the airfoil in cascade is calculated by the Kutta-Joukowski theorem (and considering $L = 4a$):

$$Cs_{cascade} = \frac{Fs}{\frac{1}{2}\rho W_\infty^2 L} = \frac{2\rho \Gamma W_\infty}{\rho W_\infty^2 L} = \frac{2\Gamma}{W_\infty L} = \frac{\Gamma}{2W_\infty a} \tag{9}$$

For isolated airfoils the following relation is approximately valid:

$$Cs_{isolated} = 2\pi \sin(\alpha + \beta^*) \tag{10}$$

But there is an analytical relation between the lift coefficients of a flat plate, isolated and in cascade, which can also be taken as an approximation (Fernandes, 1978):

$$k = \frac{Cs_{cascade}}{Cs_{isolated}}, \qquad k = \frac{4t}{\pi L}\left[\frac{R/c}{(R/c)^2 + 1}\right]\frac{\cos \theta_0}{\cos \beta}, \tag{11, 12}$$

Thus, by Eqs. (10) and (11) we have

$$Cs_{cascade} = k\,Cs_{isolated} \qquad \text{or} \qquad Cs_{cascade} = 2k\pi \sin(\alpha + \beta^*) \tag{13, 14}$$

from which one obtains the "camber angle":

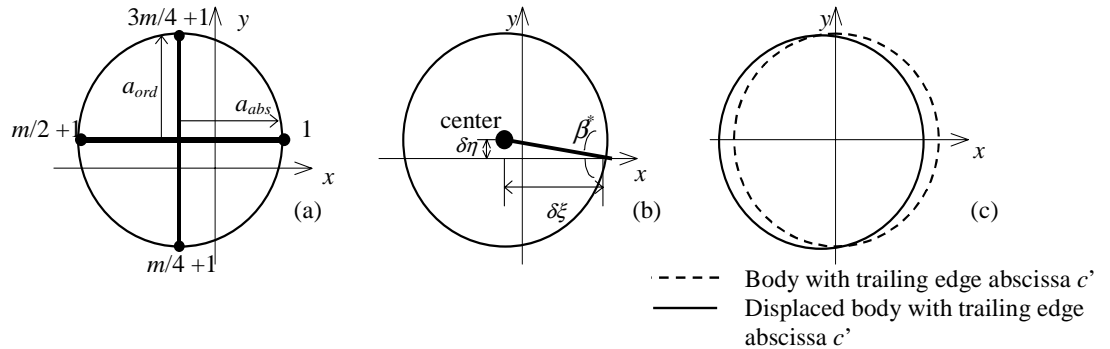$$\beta^* = \sin^{-1}\left(\frac{Cs_{cascade}}{2k\pi}\right) - \alpha \tag{15}$$

Figure 3 a) Circle radius; b) Camber angle; c) Body displacement from trailing edge abscissa c' to c.

In the first iteration, one employs the β^* calculated in Eq. (15) and considers the circle radius as unitary. In each of the subsequent iterations, new values for these parameters are computed. The radius is calculated as an average between the principal radius with respect to the abscissas and ordinates, as shown in Fig. 3. By adopting the panel number as a multiple of four, with near m/4 panels in each circle quadrant, the calculations can be simplified:

$$a_{abs} = \frac{\left|\xi(m/2+1)\right| + \left|\xi(1)\right|}{2}, \qquad a_{ord} = \frac{\left|\eta(3m/4+1)\right| + \left|\eta(m/4+1)\right|}{2}, \qquad a = \frac{a_{abs} + a_{ord}}{2} . \tag{16a,b,c}$$

The quasi-circle center is considered at the intersection of corresponding diameters. The coordinate distances $\delta\xi$ and $\delta\eta$ between the center and the rear critical point are calculated and thus the camber angle β^* directly follows (Fig. 3 b):

$$\beta^* = \arctan\frac{\delta\eta}{\delta\xi} \tag{17}$$

The new value of the critical point abscissa c is calculated by Eq. (6):

$$c = \frac{\left|W_{bf}\right| \cdot a}{W_2 \cos(\alpha + \beta^*)} \tag{18}$$

4. Flow calculation step

This step is the same as described by Petrucci et al. (2001), being implemented by means of a straight panel method with linear vortex distributions The quasi-circle contour is meshed into m straight panels with z_1, z_2, ..., z_m, z_{m+1}, representing the nodal points and $z_1 = z_{m+1}$ at the rear critical point (trailing edge), Fig. 4. The control points are chosen in the panel centers for applying the Neumann boundary condition of flow impenetrability.
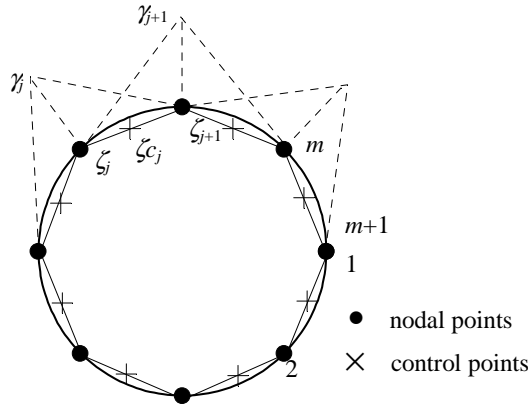

Figure 4. Panel mesh showing the nodal and control points and the nodal vortex intensities.

The complex conjugated velocity $\overline{W}_\zeta(\zeta)$ in a generic point of the complex plane $\zeta = \xi + i\eta$ follows from a Cauchy integral at the C contour, being $\zeta_c(s)$ an integration point:

$$\overline{W}_\zeta(\zeta) = \overline{W}_{\infty\zeta} + \frac{i}{2\pi}\oint_c \frac{\gamma(s)}{\zeta - \zeta_c(s)}\,ds , \tag{19}$$

where $\overline{W}_{\infty\zeta}$ is the complex conjugated velocity of the onset flow in the transformed plane, corresponding to uniform flows upstream and downstream of the cascade in the physical plane. It can be represented by suitable point source and vortex singularities at $\zeta = \pm R$, including the circulation cascade effect (Fernandes, 1978). Now, the images inside the quasi-circle are not considered anymore but must be replaced by the contour vortex distribution $\gamma(s)$ given by the panel method solution. The integral in (19) is approximated by linear vortex distributions on the straight panels. The integral contribution $\overline{W}_{\zeta j}(\zeta)$ from the nodal point z_j can be analytically calculated (χ_j is the j panel angle with respect to ξ):

$$\overline{W}_{\zeta j}(\zeta) = i\gamma_j\left\{e^{-i\chi_{j-1}}\frac{1}{2\pi}\left[\frac{\zeta - \zeta_{j-1}}{\zeta_j - \zeta_{j-1}}\log\left(\frac{\zeta - \zeta_{j-1}}{\zeta - \zeta_j}\right) - 1\right] + e^{-i\chi_j}\frac{1}{2\pi}\left[\frac{\zeta_{j+1} - \zeta}{\zeta_{j+1} - \zeta_j}\log\left(\frac{\zeta - \zeta_j}{\zeta - \zeta_{j+1}}\right) + 1\right]\right\} \tag{20}$$

Summing up all the node contributions with the onset flow velocity at the m control points and applying the Neumann boundary condition to them, a system of m panel equations for $m+1$ node unknowns, γ_j , is obtained. The Kutta condition is then applied at the trailing edge by making the system solvable. Here it is sufficient to consider γ_{m+1} $= -\gamma_1$ for causing stagnation at the rear critical point and thus satisfying correctly the Kutta condition.

5. Geometric marching step

The geometric marching step consists in modifying the panel slopes in the transformed plane in order to satisfy the conformal relations without violating the impenetrability flow condition at convergence. First, a fictitious vortex distribution is calculated from the difference between the surface velocities given by the panel method solution and the equivalent transformed velocities calculated by applying the mapping relations to the required physical velocities. This vortex distribution induces a normal velocity excess at the control points which must be annulated by suitably changing the panel slopes. Finally, a scheme for guaranteeing a closed shape is applied and a convergence test is made. If convergence is not yet attained, another iteration is carried out with the new obtained shape. In what follows these sub-steps are briefly described.

5.1. Required velocities in the transformed plane. The mapping relation between the transformed (W_ζ) and physical (W_z) complex conjugated velocities is given by

$$W_\zeta = W_z \frac{dz}{d\zeta}, \text{ with } \frac{dz}{d\zeta} = \frac{t\,e^{i\theta_0}}{2\pi}\left\{ e^{-i\beta}\left[\frac{1}{R+\zeta e^{i\theta_0}}+\frac{1}{R-\zeta e^{i\theta_0}}\right]+e^{i\beta}\left[\frac{1}{\zeta e^{i\theta_0}+c^2/R}+\frac{1}{\zeta e^{i\theta_0}-c^2/R}\right]\right\} \quad (21,22)$$
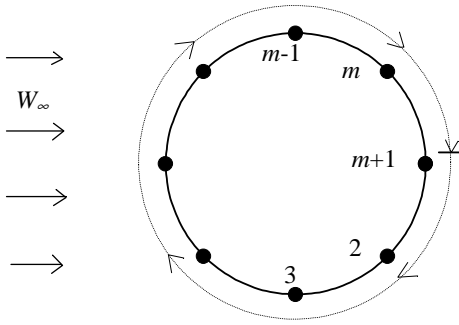

Figure 5. Adopted path orientation.

5.2. Calculation of the fictitious vortex distribution. A special care must be taken in considering the surface velocity signals of the calculated velocities, W_c, with respect to the required ones, W_r. The path orientation adopted is this work is shown in Fig. 5, by which the interior of the body is always at right. Normally there will be a stagnation point next to the leading edge such that the velocities are negative before it (intrados) and positive after it (extrados). Thus it is convenient to identify the first point for which the product between calculated and required velocities is not positive (excluding the trailing edge) an denotes this points by j_{est}, i. e.:

vary j until $W_c \cdot W_r \le 0$;   then make $j_{est} = j$ and stop the search. $\qquad (23)$

Thus, the fictitious vortex intensities γ_{fict} are calculated by the following expressions:

$$\gamma_{fict}(s) = W_c(s) - W_r(s) \qquad\qquad \text{for } j = 1, ..., j_{est} \qquad (24)$$

$$\gamma_{fict}(s) = W_r(s) - W_c(s) \qquad\qquad \text{for } j = j_{est}+1, ..., m \qquad (25)$$

5.3. Generation of a new shape. The normal velocities induced by the fictitious vortex distribution at the control points must be annulated. The j panel is rotated with respect to j node by an angle Ω_j, Fig. 6. This angle satisfies the following relations::

$$\cos\Omega_j = \frac{\left|W_{r\zeta}\right|}{\sqrt{W_{r\zeta}^2 + W_n^2}} \;;\qquad \text{sen}\,\Omega_j = \frac{W_n}{\sqrt{W_{r\zeta}^2 + W_n^2}} \qquad (26a, b)$$

The complex elementary increments before and after rotation ($d\xi + id\eta$ and $d\Xi + id\mathrm{H}$ respectively) are related by

$$d\Xi + id\mathrm{H} = (d\xi + id\eta)e^{i\Omega} \tag{27}$$

The first node at trailing edge is fixed, $j = 1$; the new coordinates of the $j+1$ node are given by an approximated integration of Eq. (27):

$$\Xi_{j+1} = \Xi_j + \cos\Omega_j(\xi_{j+1} - \xi_j) - \sin\Omega_j(\eta_{j+1} - \eta_j) \tag{28}$$

$$\mathrm{H}_{j+1} = \mathrm{H}_j + \sin\Omega_j(\xi_{j+1} - \xi_j) + \cos\Omega_j(\eta_{j+1} - \eta_j) \tag{29}$$
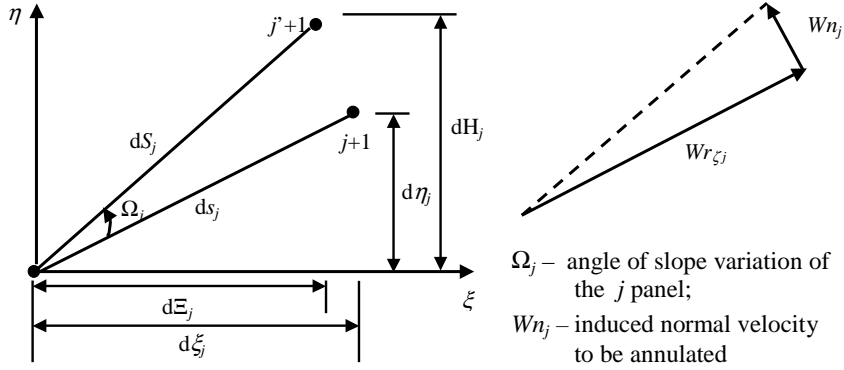
Figure 6. Variation of panel slope .

5.4. Coordinate Reposition. The panel lengths $\Delta S_{req\zeta}$ in the transformed plane must be in accordance with the required lengths at the physical plane, ΔS_z, by the conformal mapping relation:

$$\Delta S_{req\zeta_j} = \Delta S_{z_j} \cdot \left|\frac{dz}{d\zeta}\right|_{\zeta c_j} \tag{30}$$

But after modifying the panel slopes, we obtain new panel lengths $\Delta S'_{\zeta_j}$ that do not necessarily agree with the required values given by Eq. (30). Thus, it becomes necessary to perform a coordinate reposition of the node points in order to satisfy this conformal mapping requirement. The repositioned coordinates $(\Xi', \mathrm{H}')_j$ are calculated by the following adjustment relations:

$$\Xi'_{j+1} = \Xi'_j + (\Xi_{j+1} - \Xi_j)\frac{\Delta S_{req\zeta_j}}{\Delta S'_{\zeta_j}}, \qquad \mathrm{H}'_{j+1} = \mathrm{H}'_j + (\mathrm{H}_{j+1} - \mathrm{H}_j)\frac{\Delta S_{req\zeta_j}}{\Delta S'_{\zeta_j}} \tag{31a, b}$$

5.5. Scheme for the body closure. Even after the coordinate reposition, the resulting body shape may still be not closed at the trailing edge as required, i. e., one can have $\zeta_{m+1} \neq \zeta_1$. To overcome this situation, a correction scheme for closing the body shape is applied. The scheme consists in proportionally distribute the coordinate difference $\zeta_{m+1} - \zeta_1$ among the panel nodes $j = 2, 3, ..., m+1$, starting from the fixed trailing edge $j = 1$. The coordinates $(\tilde{\Xi}, \tilde{\mathrm{H}})_j$ of the desired closed body are so calculated by the following relations:

$$\tilde{\Xi}_{j+1} = \Xi'_{j+1} + j \cdot \frac{\Xi'_1 - \Xi'_{m+1}}{m}, \quad \tilde{\mathrm{H}}_{j+1} = \mathrm{H}'_{j+1} + j \cdot \frac{\mathrm{H}'_1 - \mathrm{H}'_{m+1}}{m} \tag{32a, b}$$

5.6. Stopping criteria of the iterative process. The convergence criteria adopted in this work is based on the mean quadratic deviation between the ordinates calculated in two subsequent iterations. The iterative process is stopped when that deviation rests below a stipulated tolerance, ε:

$$\left(\frac{1}{m}\sum_{j=1}^{m+1}\Delta\tilde{Y}_j^2\right)^{1/2} \leq \varepsilon \tag{33}$$

where $\Delta \tilde{Y}_j$ represents the difference between the body ordinates $\tilde{Y}_j$ calculated in the present and anterior iterations.

The target shape coordinates in the physical plane z are calculated from the coordinates of the converged quasi-circle in the transformed plane ζ by directly applying the conformal mapping relation, Eq. (2).

6. Methodology validation

In order to validate the proposed hybrid approach for cascade inverse design, some benchmark tests were carried out. Three representative examples will be presented here: 1) a Weinig cascade, obtained from a circle in the transformed plane and for which a preliminary test can be made; 2) a cascade composed of Joukowski airfoils for which there is no available analytical solution for a finite pitch; 3) the Gostelow cascade (1984), for which an analytical solution is available but not via the Weinig conformal mapping. For the Weinig cascade, the required velocity distribution correspond exactly to the analytical one. For the cascade of Joukowski airfoils, the required velocity distribution was numerically stipulated by applying the panel method to the target cascade directly in the physical plane. For the Gostelow cascade, a cubic spline interpolation was applied on the tabulated data given by Gostelow (1984) in order to specify the required velocity values for a convenient set of nodal points on the contour.

The following results are presented in each test example: 1°) the iterative geometrical evolution in the transformed plane (quasi-circle); 2°) the iterative geometrical evolution in the physical plane (airfoil); here, the ordinate scale is amplified for better visualization; 3°) the iterative evolution of the velocity distribution in the physical plane; 4°) an amplification of the leading edge region. In all of the examples, a converge tolerance equal to 10^{-4} was adopted.

Example 1 – Target: Weinig cascade with cambered airfoils; geometrical and kinematical parameters: $a/me = 4,5$, $\beta^* = 8°$, $\beta_\infty = 34°$, $\beta = 30°$, $t/L = 1$, $\alpha = 4°$. Panel number: $m=24$.
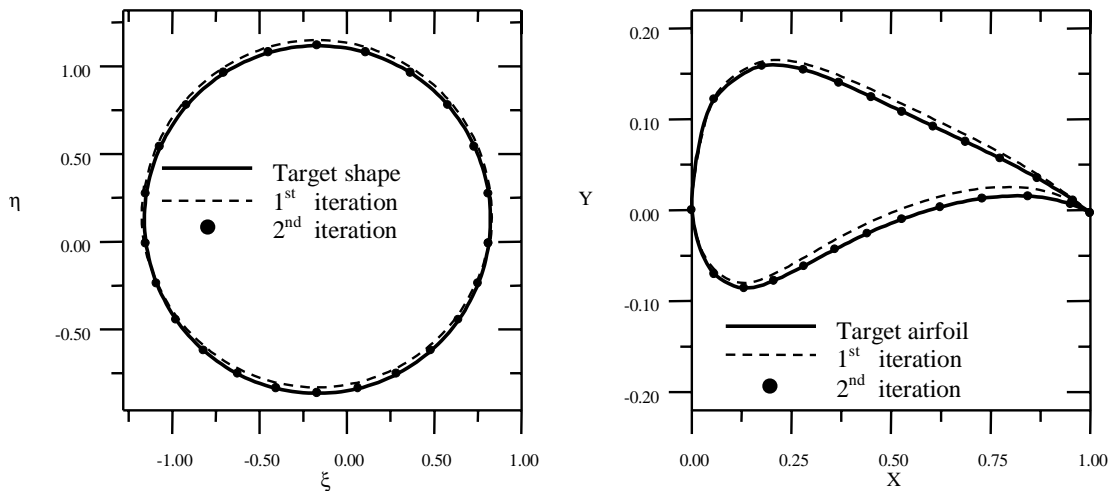

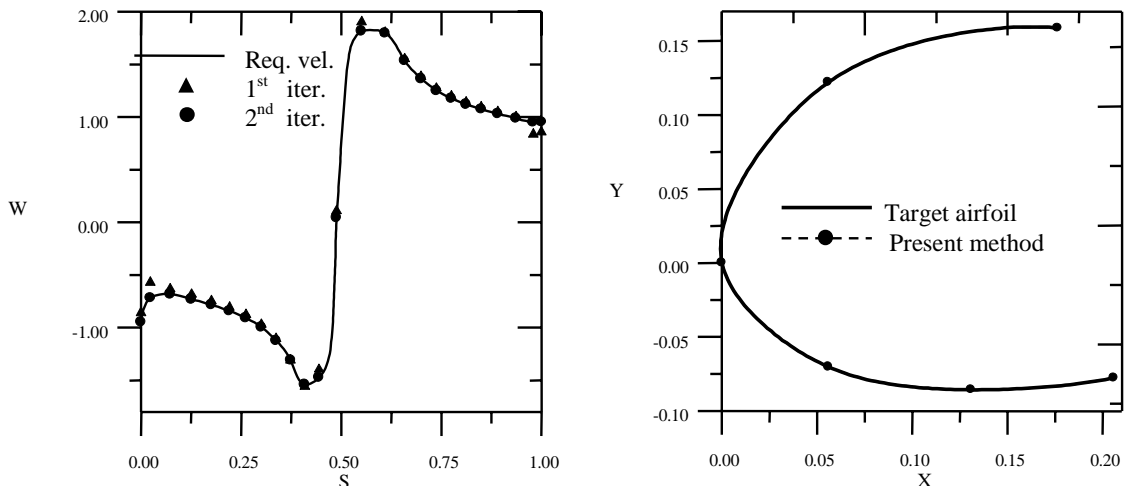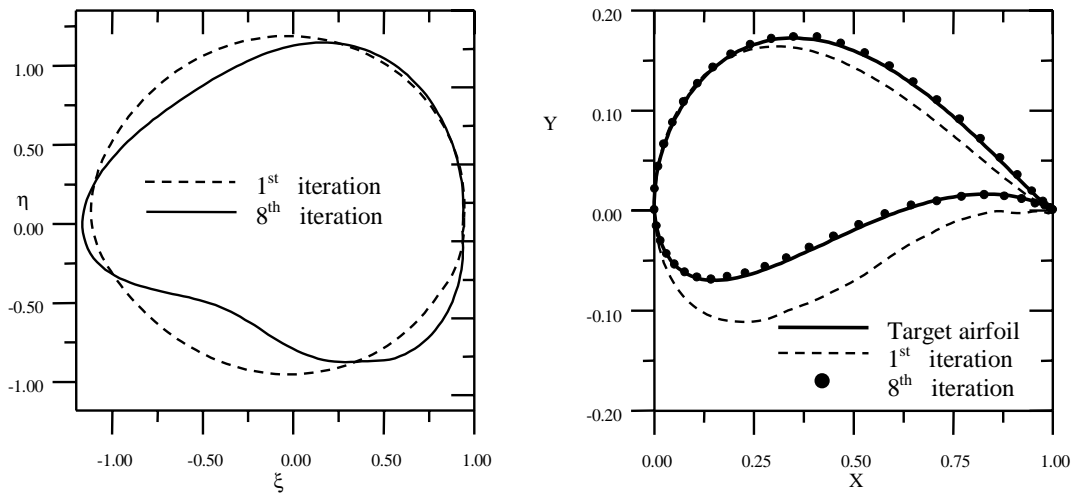Figure 7 – Example 1- iterative geometrical evolution. a) transformed plane; b) physical plane.

Figure 8 – Example 1: a) velocity evolution in the physical plane; b) amplification of the leading edge region.

Exemple 2 – Target: cascade of cambered Joukowski airfoils; geometrical and kinematical parameters: $a/me =$ 4,5 , $\beta* = 8°$ (for the Joukoswki mapping,), $\beta_\infty = 30°$, $\beta = 30°$, $t/L = 1$, $\alpha = 0°$. Panel number $m=50$.

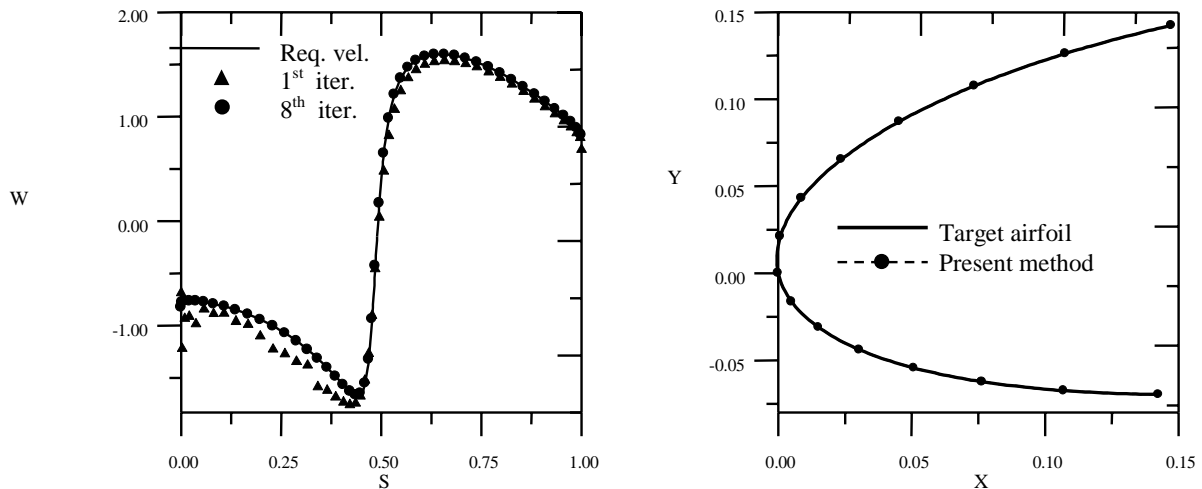Figure 9 – Example 2: iterative geometrical evolution. a) transformed plane; b) physical plane.

Figure 10 – Example 2: a) velocity evolution in the physical plane; b) amplification of the leading edge region.

Example 3 – Target: Gostelow cascade; geometrical and kinematical parameters: $\beta = 37,5°$, $t/L = 0,9901573$, $\beta_\infty = 43,968°$, $\alpha = 6,468°$. Panel number: $m = 50$.
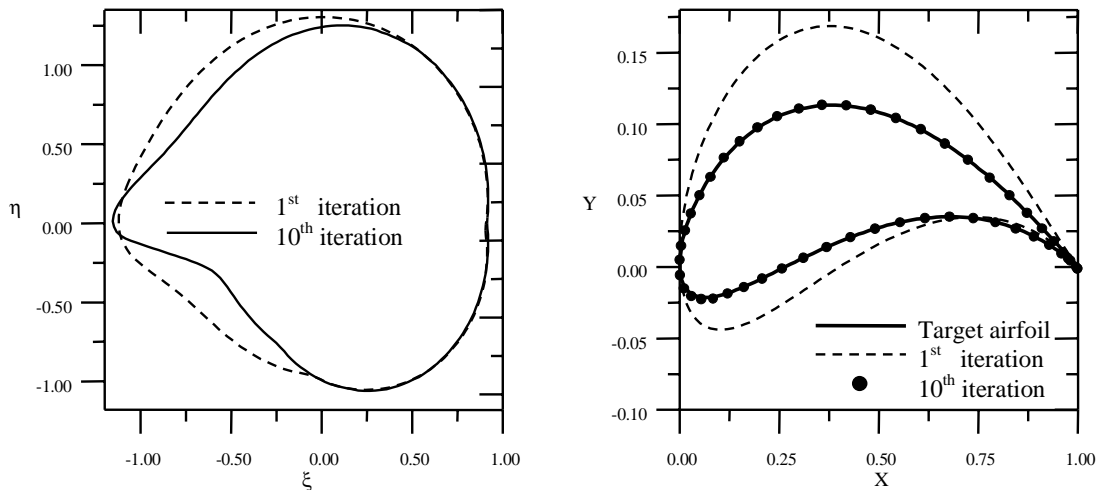

Figure 11 – Example 3: iterative geometrical evolution. a) transformed plane; b) physical plane.
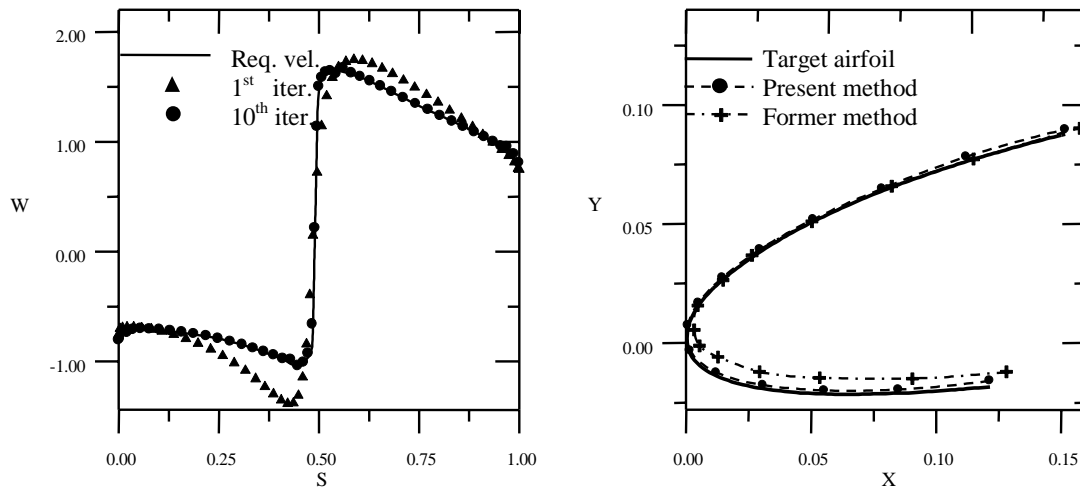
Figure 12 – Example 3: a) velocity evolution in the physical plane; b) amplification of the leading edge region.

In all of the tests, convergence was attained with a small number of iterations. For the Weinig cascade (Figs. 7 and 8), only 2 iterations were necessary. It could be argued that only one iteration would really suffice in this case, since the inverse approach uses the own Weinig mapping and thus the starting shape would already be the target shape in the transformed plane. But this is not exactly true, since the procedures adopted for computing the mapping parameters are only approximated and the inverse approach must eliminate the small differences at start by its own. It is interesting to note that for isolated Joukowski airfoils the procedures become exact and only one iteration would be necessary (Petrucci and Manzanares, 2002 a). Nevertheless it is important to remember that the required velocities are purely analytical in this example while the flow calculation step is not exact (panel method). Thus, this first example can be considered as a successful preliminary test for the methodology consistency. On the other hand, for the cascade of cambered Joukowski airfoils (Figs. 9 and 10) and the Gostelow cascade (Figs. 11 and 12), 8 and 10 iterations were necessary for convergence, respectively. But one has still a quite rapid and precise convergence process capable of capturing all the required smoothness of the target shape contour, particularly at the leading edge region (Figs. 8b, 10b and 12b). This aspect is of a rather practical importance when considering the geometric requirements for wing and blade manufacturing.

The test results can be considered as very satisfactory when compared with corresponding results obtained by a former method presented by Petrucci and Manzanares (2002 b). That method did not employ conformal mappings and required some heuristic procedures for accelerating the convergence process. But even taking this care, the number of iterations for convergence was significantly larger than by the present method (from 2 to 6 times more iterations). Also the converged results obtained at the leading edge region were not as satisfactory as that obtained by the present method (Fig. 12b). This comparison indicates that the inverse hybrid approach combining a conformal mapping and a efficient panel method actually constitutes a suitable approach for cascade airfoil design.

7. Conclusions

In this work, an hybrid methodology for inverse airfoil design of turbomachinery cascades was presented. The technique combines the Weinig conformal mapping and a straight panel with linear vortex distributions.

The methodology was validated by various test examples and three of them were presented in this paper. In all of the tests, it was possible to obtain target aerodynamic shapes more rapidly an more precisely in comparison with another inverse algorithm previously presented by the authors (Petrucci and Manzanares, 2002 b). Besides the satisfactory smoothness obtained in the leading edge region, the hybrid technique have dispensed some heuristic procedures of the former algorithm for accelerating the convergence process.

The test results have demonstrated the good versatility and precision of the methodology in obtaining target cascade airfoils with few iterations (typically ≤ 10) and a small number of panels (24 to 50). These are important issues when considering the inclusion of viscous effects in the flow calculation step. For viscous flow models, the computation time per iteration can increase orders of magnitude compared with the time needed to solve a potential flow model. Thus it is important for the inverse algorithm to converge with a number of iterations as small as possible.

8. Acknowledgments

9. Bibliographic References

Dulikravich, G.S. (1992), "Aerodynamic Shape Design and Optimization: Status and Trends ", J. Aircraft, Vol. 29, No. 6, pp. 1020-26.

Fernandes, E. C. (1978), "Analysis of Turbomachinery Flows by the Singularity Method " (in Portuguese), Instituto Tecnológico de Aeronáutica – ITA, São José dos Campos, SP, Brazil.

Gostelow, J. P., 1984, "Cascade Aerodynamics ", Pergamon Press Ltd..

Karamcheti, K., 1980, "Principles of Ideal-Fluid Aerodynamics ", R. E. Krieger Publishing Company, Florida.

Liu, G.L. (1995), "Advances in Research on Inverse and Hybrid Problems of Turbomachinery Aerothermodynamics in China", Inverse Problem in Engineering, Vol. 2, No. 1, pp. 1-27.

Liu, G. L. (2000), "A New Generation of Inverse Shape Design Problem in Aerodynamics and Aerothermoelasticity: Concepts, Theory and Methods", Aircraft Engineering and Aerospace Technology: An International Journal, Vol. 72, No 4, pp. 334 – 344.

Milne-Thomson, L. M., 1966, "Theoretical Aerodynamics", Dover Publications, INC., New York.

Murugesan, K., Railly, J. W., 1969, "Pure Design Method For Aerofoils in Cascade", Journal of Mechanical Engineering Science, vol. 11, No. 5, pp. 454-467.

Petrucci, D., R., 1998, "Inverse Problem of The Flow Around Isolated Airfoils or Turbomachinery Cascades" (in Portuguese), MSc. Dissertation, Universidade Federal de Itajubá, Itajubá, MG, Brazil.

Petrucci, D. R., Manzanares Filho, N., Ramirez, R. G., 2001, "An Efficient Panel method Based on Linear Vortex Distributions for Analysis of Turbomachinery Cascade Flows" (in Portuguese), XVII Brazilian Congress of Mechanical Engineering (COBEM 2001), CD-ROM Proceedings, Uberlândia, MG, Brazil.

Petrucci, D. R., Manzanares Filho, N., 2001, "A Fast Algorithm for Inverse Airfoil Design Using Panels with Linear Vortex Distributions", 22nd Iberian Latin-American Congress on Computational Methods In Engineering - 2nd Brazilian Congress on Computational Mechanics (XXII CILAMCE), CD-ROM Proceedings, Campinas, SP, Brazil.

Petrucci, D. R., Manzanares Filho, N., 2002 a, "An Hybrid Technique for Inverse Airfoil Design Using Conformal Mapping and The Panel Method" (in Portuguese), IX Brazilian Congress of Engineering and Thermal Sciences (ENCIT 2002), Paper CIT02-0232, CD-ROM Proceedings, Caxambu, MG, Brazil.

Petrucci, D. R., Manzanares Filho, N., 2002 b, "A Method for Airfoil Design of Turbomachinery Cascades Using Iterative Correction" (in Portuguese), IX Brazilian Congress of Engineering and Thermal Sciences (ENCIT 2002), Paper CIT02-0438, CD-ROM Proceedings, Caxambu, MG, Brazil.

Selig, M. S., Maughmer, M. D., 1992a, "Multipoint Inverse Airfoil Design Method Based on Conformal Mapping ", AIAA Journal, vol. 30, No 5, pp. 1162-1170.

Selig, M. S., Maughmer, M. D., 1992 b, "Generalized Multipoint Inverse Airfoil Design ", AIAA Journal, vol. 30, No 11, pp. 1162-1170.

Selig, M. S., 1994, "Multipoint Inverse Design of an Infinite Cascade of Airfoils ", AIAA Journal, vol. 24, No 4, pp. 774-782.

Shigemi, M., 1985, "A Solution of an Inverse Problem For Multi-Element Aerofoils Through Application of Panel Method", Trans. Japan Soc. Aero. Space Sci., vol. 28, No. 80, pp. 97-107.

Yiu, K. F. C., 1994, "Computational Methods for Aerodynamic Shape Design", Mathematical and Computer Modelling, vol 20, No. 12, pp. 3-29.